Nuclear Instruments and Methods in Physics Research B 332 (2014) 207–211

Contents lists available at ScienceDirect

Nuclear Instruments and Methods in Physics Research B

journal homepage: www.elsevier.com/locate/nimb

The implementation of a DSSSD in the upgraded boron analysis at LIBAF for applications in geochemistry

P. Kristiansson [a,*], M. Borysiuk [a], U. Hålenius [b], J.L. Mosenfelder [c], L. Ros [a], H. Skogby [b], N. Abdel [a], M. Elfman [a], E.J.C. Nilsson [a], J. Pallon [a]

[a] Division of Nuclear Physics, Department of Physics, Lund University, Lund, Sweden
[b] Swedish Museum of Natural History, Department of Geosciences, Stockholm, Sweden
[c] Caltech, Division of Geological and Planetary Sciences, Pasadena, CA, USA

ARTICLE INFO

Article history:
Available online 24 March 2014

Keywords:
Boron analysis
NRA
(p,3α)-Reaction
DSSSD

ABSTRACT

Interest in high spatial resolution boron analyses from a geochemical perspective is related to the recognition of boron as an important tracer of chemical recycling in the Earth, due to the high solubility of boron in aqueous fluids and silicate melts. Although boron is not a nominal component in common silicates they may still contain significant B-concentrations and hence constitute important boron reservoirs in the deeper parts of the Earth.

Boron analyses have been performed at the Lund Ion Beam Analytical Facility for almost 20 years. For the analysis the nuclear reaction p+^{11}B is used with beam energy just below 700 keV where the reaction has a broad resonance.

In this paper we describe an upgrade of the system with a double sided silicon strip detector, which allows for much higher count rates compared to the old annular surface detector based system. A gain close to 20 in the data rate allows for high resolution mapping of boron distributions in crystals. This is illustrated by a number of examples. In addition, the detection limits for boron in geological samples are improved, now around 5 ppmw. In this work we address issues with data quality, especially charge normalization, lifetime correction and subtraction of different background components.

1. Introduction

Boron related analyses have been performed at LIBAF (Lund Ion Beam Analysis Facility) for almost 20 years. For the analysis the nuclear reaction p+^{11}B is used with beam energy just below 700 keV, where the reaction has a broad resonance. This reaction emits three alpha particles with energies much higher than the elastically scattered proton, which can easily be discriminated and counted as a function of beam charge. The focus of initial application was on analysis of boron distribution in cell tissue for BNCT (Boron Neutron Capture Therapy) [1], but soon interest shifted towards geoscience and boron analysis in crystals, both synthetic and natural [2,3]. To detect the alpha particles, an annular surface barrier detector was used with a focused ion beam and analysis currents below one nA. This kept the total count rate in the detector below 10 kHz, which was considered acceptable for this kind of analysis. In this paper we will describe and evaluate the upgrade of the system from a single detector to a segmented silicon detector. This upgrade substantially increases the possibility to work with much higher total count rates, hence reducing the time for analysis or alternatively increase the statistics needed for imaging and improving detection limits (MDL). The capability will be illustrated by two sets of geological samples further described in Section 2.

Interest in high spatial resolution boron analyses from a geochemical perspective is related to the recognition of boron as an important tracer of chemical recycling in the Earth, as a result of the high solubility of boron in aqueous fluids and silicate melts. Although boron is not a nominal component in common silicates (e.g. pyroxene, olivine, sillimanite) they may contain enhanced B concentrations ($\leqslant$1 wt.% B_2O_3) and hence constitute important boron reservoirs in the deeper parts of the Earth [4]. The nature of B substitution mechanisms in these minerals is not fully understood and partly contradictory models have been suggested.

Measurements of hydrous B-bearing minerals (e.g., tourmaline, muscovite, and illite), melts and aqueous fluids suggest that

* Corresponding author. Address: Lund University, Department of Physics, Nuclear Physics, P.O. Box 118, SE-221 00 Lund, Sweden. Tel.: +46 46 222 76 27, mobile: +46 70 317 24 01.
E-mail address: per.kristiansson@nuclear.lu.se (P. Kristiansson).

http://dx.doi.org/10.1016/j.nimb.2014.02.062
0168-583X/

isotopic fractionation of boron is strongly dependent on how boron is coordinated by its nearest anions [5].

^{10}B has a marked preference for the tetrahedral BO_4 configuration, while ^{11}B prefers the trigonal BO_3-groups. It has generally been assumed in geochemical models that boron is tetrahedrally coordinated when present at low levels in silicate minerals of mantle affinity and that fluid phases coexisting with these silicates contain BO_3-groups. Consequently, ^{11}B would show a strong partitioning into the fluid phase. However, recent studies on synthetic equivalents of the clinopyroxene mineral have demonstrated that B^{3+} substitution for Si^{4+} involves replacement of SiO_4-groups with BO_3-groups, with charge balance retained through coupled substitutions involving vacancy formation [6].

With the aim to explore whether natural olivine and clinopyroxene also preferentially incorporate BO_3-groups, we have conducted a preliminary study involving ^{11}B NRA to select suitable specimens for subsequent spectroscopic FTIR- and NMR-based studies. If this is the case, conclusions drawn from boron isotope studies under the assumption of an exclusive presence of BO_4 groups in mantle minerals may need reconsideration. The main objective of the study is to explore the boron exchange mechanisms in silicate minerals as they are of fundamental importance for understanding the large-scale geochemical cycle of boron.

2. Experiment

The experiment was performed at the Lund Ion Beam Analysis Facility [7,8] at the sub-micron beam line. The accelerator, a 3 MV NEC Pelletron had one section shorted and produced beams of 700 or 610 keV protons. The beam was transported through the standard slit package and projected onto a quartz plate for focusing. The beam spot size and the scanning step length were evaluated by irradiating a 300 mesh Cu-grid to 5 μm and 1.5 μm respectively. A typical scan was 128*128 pixels with a step length of 8*1.5 μm. The typical beam current used was 5 nA.

The detector used during the experiment was a DSSSD (Double-Sided Silicon-Strip Detector) with 64 sectors on the front side and 32 rings on the back side, i.e. in total 2048 detector element formed by the crossing of sectors and rings. Typical detector parameters for the setup are solid angle coverage of about 3.5 sr and resolution of 35 keV measured with a ^{228}Th-source. The introduction of many more detector channels will reduce the count rate per strip and hence remove the limitation on beam current for the single detector set-up. This system is described in detail in reference [9]. For the present experiment the electronics was adjusted to maximize the observed yield of the interesting B reaction. The thresholds were set as low as possible on the separate ring signals (from the back-side) while high thresholds were set on the sector signals. The high threshold signal was used both to discriminate elastically scattered particles and also pile-up in single sectors. The low threshold signal was used as count rate signal for imaging and this in coincidence with the high threshold signal was used to identify boron events.

Data were acquired using a combination of the old CAMAC based system for scanning and the new VME [10] based system for energy spectroscopy. At the time of the experiment the scanning capability had not been fully implemented in the new VME system. Due to the hard trigger conditions the acquisition could be run with very high live time, about 95%.

The capability of the upgraded system is illustrated by analyses of two sets of geological samples. One set was placed on an indium backing, high Z and non-transparent, while the other was placed in an epoxy mount with glass backing, low Z and transparent. Each mount had between 15 and 20 crystals plus a tourmaline crystal [3] included as a standard for normalization. The measured crystals have concentrations ranging up to 5000 ppmw (ppm by weight) BO_3, with hot spot concentrations much higher. There are examples of both homogeneous crystals and crystals with zonation patterns.

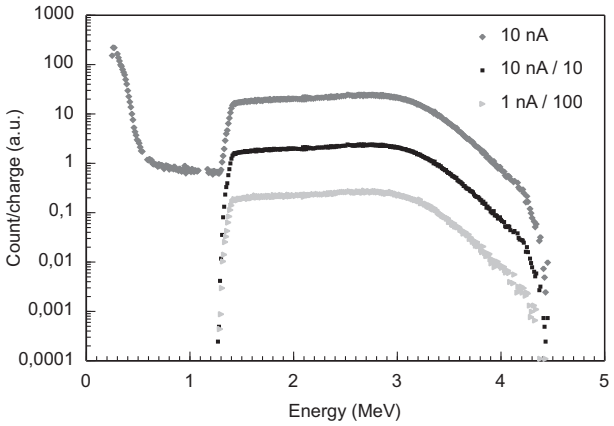

Fig. 1. Spectra showing data from two different runs on a tourmaline standard with different beam currents, approximately 1 and 10 nA. The data sets are normalized to beam charge and corrected for live time. Each consecutive spectrum is scaled a factor of 10 for presentation purposes. A detailed description of the figure is given in the text.

There are two possible options for normalization for the setup, either a pre-sample deflection system [11] for charge measurement or an internal standard relative measurement. The advantage with the pre-sample system is that it is totally sample independent, whereas the internal standard system allows for both charge and count-rate normalization. During this experimental run the internal standard technique was utilized.

3. Results

The different backings of the two sample mounts (one high Z and one low Z) required different experimental conditions for the analysis, particularly for imaging. In addition to the data acquired for geoscience purposes the internal tourmaline standards mounted with the samples were used for evaluation of the upgraded system with the new DSSSD detector.

3.1. System evaluation – Energy distributions

Energy spectra from tourmaline standards obtained under different conditions are shown in Figs. 1–3. The upper curve in Fig. 1 is the raw spectrum taken with a current of about 10 nA

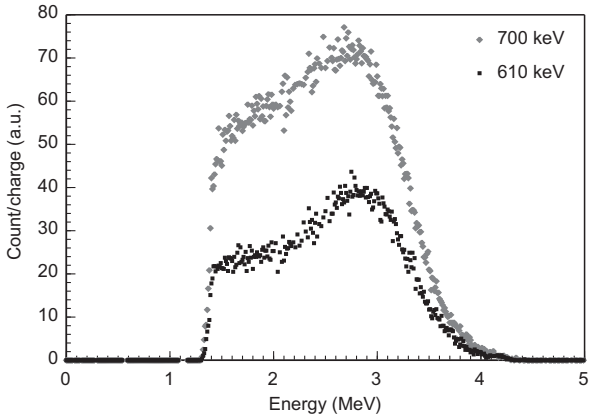

Fig. 2. Two spectra from a tourmaline standard collected with two different beam energies, 610 keV (bottom) and 700 keV (top). The difference in yield is about a factor of two, as expected from cross-section data.

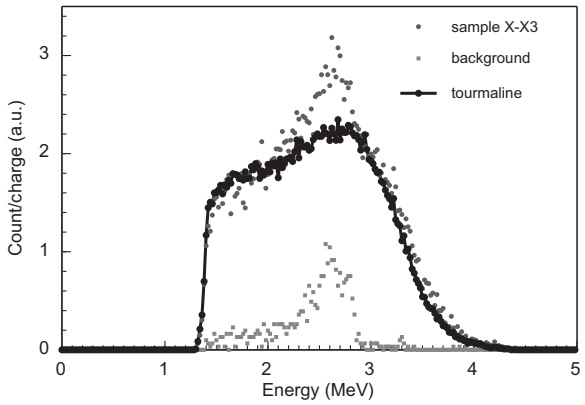

Fig. 3. Spectra from an olivine crystal with a relatively low boron concentration (top) and a boron free crystal (bottom) used as background. To guide the eye a tourmaline spectrum has been scaled and overlaid on the spectrum from the boron-containing crystal and the additional back ground component is clearly seen.

and the second curve (scaled down by a factor of 10 in the figure) is the same set of data but gated using multiplicity condition one from the DSSSD detector. In this case the requirement is that one and only one of the rings have a signal over the threshold. This condition cleans out much of the background at low energies and the high-energy threshold set on the sector side appears even sharper. The third curve, scaled down by a factor of 100, is a spectrum of the same sample but taken with a beam current ten times lower. The shape and the total normalized yield for all three spectra is the same showing that the system has a very high total count rate capability before it deviates from linearity.

As mentioned previously the reaction $^{11}B(p,2\alpha)\alpha$ has a very broad resonance with a bell shaped maximum around 630 keV. This is partly illustrated by the two energy distributions in Fig. 2. The top curve (700 keV) can be interpreted as an integral over a large part of the reaction peak, while the lower curve simply uses data from the low energy side of the peak and for the settings used here gives roughly half of the yield. One reason to choose the energies in this way is that at the higher energy a well-known p+^{18}O resonance interferes with the boron peak while at the lower energy the beam is below this resonance.

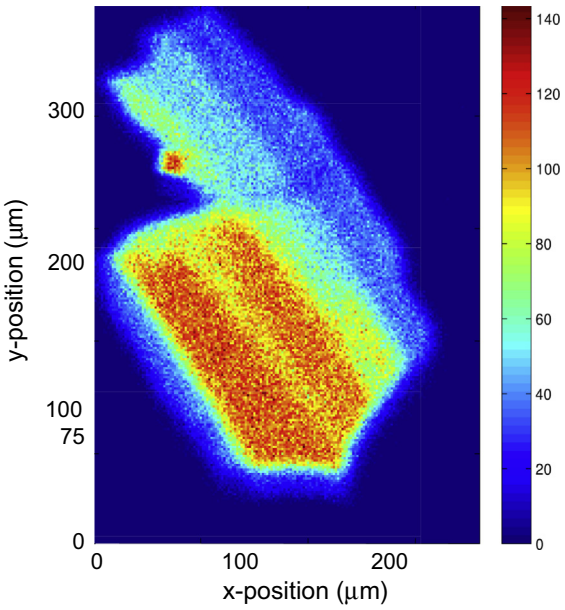

Fig. 4. High resolution map of boron on a sillimanite crystal clearly showing the zonation pattern in the crystal. The step length was 1.5 μm.

In Fig. 3, a background spectrum (with boron concentration below the detection limit) and one spectrum from a relatively low boron concentration crystal are shown (X-X3 from the Table 1). The solid line is from the tourmaline yield scaled to the boron concentration in X-X3. The overlay of background on the boron distribution in the measurement is clearly visible. Integrating the background spectrum gives a value of roughly 150 ppmw B_2O_3 corresponding to approximately 47 ppmw boron.

The background will be lower if beam energies below the ^{18}O resonance are used, but so will the yield for a fixed charge. To give an idea of the detection limits that can be achieved, we assume the criterion that the minimum detection limit (MDL) corresponds to three times the square root of the background signal. Using the number of counts from Table 1 (36034X2) the detection limit for

Table 1
The table shows a typical protocol from an experiment for quantitative boron analysis, in this case the set of natural Mg-rich olivine crystals. Each crystal in the set is mapped for boron, and for each map, one or many regions are selected where boron and charge normalisation numbers are extracted. The data is then normalized, lifetime corrected and the background is subtracted. Finally, the reference sample (tourmaline) is used to convert data to ppm concentration of B_2O_3. Not shown in the table is the last step where SRIM is used to volume correct the data [3].

Kmax run No.	VME Run No.	Sample	Comment	*I* (nA)	B-counts	No of pixel *B*	Q (B-area)	*B*/*Q*	Live time (%)	B/Q - bkg	Err	Norm (ppm) B_2O_3	Stat err
16	544	Tourm.	Reference		533106	3774	45686	11.669	96	11.6506	0.0160	***101800***	**140**
17	545	20425X2		1.9	38132	4407	165979	0.230	97	0.2114	0.0012	**1832**	**11**
18	546	20425X1	Mean	3.5	27660	8012	182717	0.151	96	0.1331	0.0010	**1166**	**8**
		20425X1	High *B* part		7384	1494	34140	0.216	96	0.1980	0.0026	**1734**	**23**
19	547	20441X1		2.3	29181	2312	240602	0.121	90	0.1030	0.0008	**958**	**7**
20	548	20441X2		3.6	38374	5740	328941	0.117	95	0.0984	0.0006	**867**	**6**
21	549	36034X1	No boron		4303	14882	223091	0.019	97	0.0010	0.0004	**9**	**4**
22		36034X2	No boron	3.7	3446	3922	190212	0.018	97	−0.0002	0.0004	**−2**	**4**
23		27122X1		1.2	13296	2355	65496	0.203	97	0.1847	0.0018	**1602**	**16**
24	552	27122X2		1.8	10418	3639	82866	0.126	97	0.1074	0.0013	**928**	**11**
25	553	90123X2	No boron	2.3	4049	5952	237318	0.017	95	−0.0012	0.0004	**−11**	**3**
26		74591X1	No boron	3.6	12643	3718	72674	0.017	95	−0.0008	0.0002	**−7**	**2**
27	555	74591X2	No boron	3.0	4695	4864	257522	0.018	96	−0.0001	0.0004	**−1**	**3**
28	556	99011X1		2.8	22657	9479	444452	0.051	96	0.0327	0.0004	**286**	**3**
29	557	99011X2		2.7	7380	8954	160725	0.046	97	0.0276	0.0006	**240**	**5**
30	558	X-X3		2.9	190750	6060	813929	0.234	97	0.2161	0.0006	**1881**	**5**
31	559	X-X2		3.1	81370	5827	339848	0.239	96	0.2211	0.0009	**1929**	**8**
32	560	X-X1		2.9	35767	4549	150026	0.238	94	0.2201	0.0013	**1961**	**12**

The final results and errors are marked bold and the reference sample with italic.

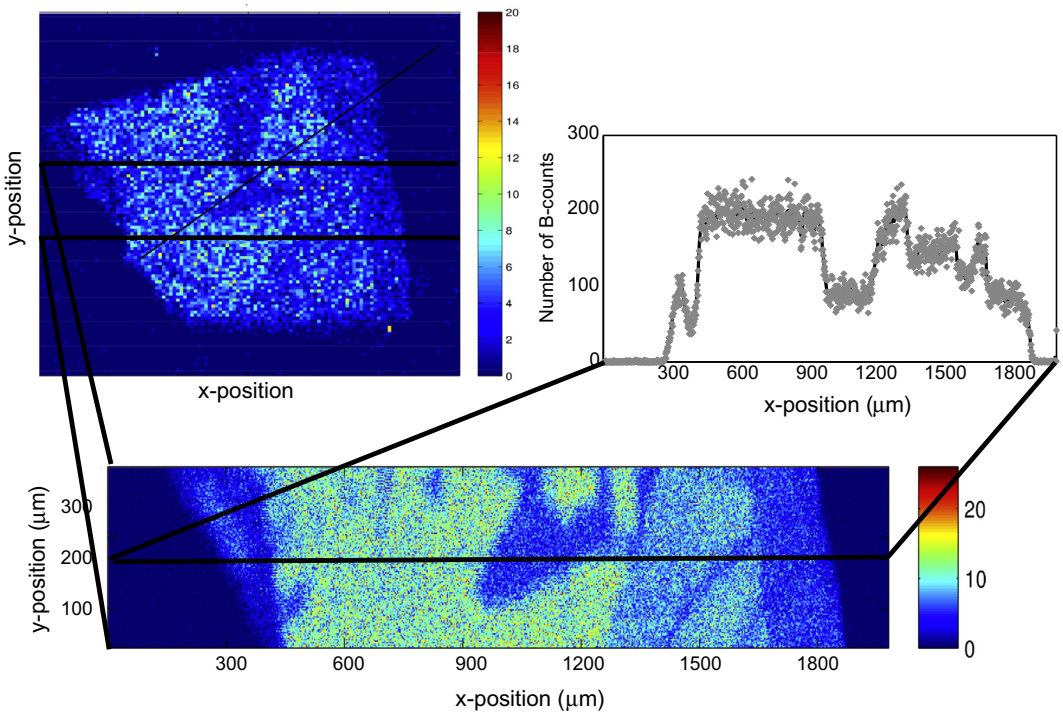

Fig. 5. An illustration of how, high resolution data can be extracted quantitatively. A coarse map is scanned (top left). From this data, the interesting region is defined and scanned with much higher lateral resolution, here in 3 μm steps (bottom). Finally, a maximum resolution profile can be collected (1.5 μm step), which then easily can be used to study variations in concentrations.

boron will range from 2 to 10 ppmw when varying the time of analysis from 2 h down to 5 min.

The main component in the background when analyzing geological materials is the contribution from ^{18}O since oxygen is a major component in most minerals or glasses of interest. The major element composition of the sample can be obtained by methods such as PIXE or SEM and the amount of oxygen calculated can then be used to predict the expected variation in background for different crystals, assuming constant (i.e. natural) ratios for the oxygen isotopes.

3.2. Mapping

For the mapping illustration two crystals of sillimanite (Al_2SiO_5) from the indium-backed mount were selected. In Fig. 4 an illustration of what can be achieved with a high lateral resolution run with good statistics is shown. The zonation pattern in the crystal can be clearly seen in the figure.

Fig. 5 demonstrates another application of the scanning method. A fast scan gives the gross features of the crystal. Then an area is selected, the step size is decreased and a high-resolution map over the interesting part of the crystal is collected. Finally a line scan is performed with optimal resolution.

3.3. Quantitative analysis

Quantitative analysis is the primary goal of the presented technique. In the Table 1 the different steps going from yield to ppmw are illustrated for the olivine samples mounted in epoxy. First a suitable area from a scan is selected and the number of B-counts is extracted from this area. The corresponding charge is extracted and used to normalize the data. Finally the background is subtracted and the concentration is normalized to the tourmaline standard.

The geological conclusions from the quantitative analysis and the mapping information will be discussed elsewhere.

4. Summary and conclusion

To summarize, the upgraded boron analysis setup at LIBAF has been discussed. The setup is upgraded with a new, segmented DSSSD with 2048 detector cells formed by 96 channels replacing one single annular SBD. The count rate capability increased drastically from about 10 kHz to above 200 kHz, which implies that the data rate from the boron signal increased a factor of 20. No effects of spectral degradation due to high count-rate could be observed.

The system has been tested by analyzing two sets of geological crystals with boron concentrations in the range up to the%-level. The increased data flux implies better detection limits and also the possibility to do high-resolution boron mapping which has been illustrated by two examples. Background and the influence of different types of background on data and detection limits have been discussed. A typical MDL would be around 5 ppmw for boron.

In the future a fixed installation of the boron setup will be possible improving the capability and the access to fast analysis. The recent development in the setup for photon-tagged Nuclear Reaction Analysis (pNRA) [12] opens up the option to do boron isotope measurements, for example by complementing the present technique on ^{11}B with a (p,α)-reaction on ^{10}B [13]. This would be of geochemical interest since ^{10}B has a marked preference for the tetrahedral BO_4-configuration, while ^{11}B prefers trigonal BO_3-groups.

Acknowledgement

The support from the Swedish Research Council (VR) is acknowledged.

References

[1] K.A. Sjöland, P. Kristiansson, M. Elfman, K.G. Malmqvist, J. Pallon, R.J. Utui, C. Yang, Subcellular analysis of boron with a nuclear microprobe, Nucl. Instrum. Meth. B 129 (1997) 101.

[2] P. Kristiansson, U. Hålenius, H. Skogby, M. Elfman, K. Malmqvist, J. Pallon, Boron distributions in single crystals investigated with nuclear reaction micro analysis, Nucl. Instrum. Meth. B 158 (1999) 562.

[3] H. Skogby, P. Kristiansson, U. Hålenius, An assessment of nuclear microprobe analyses of boron in silicate minerals, Am. Mineral. 88 (2003) 1601–1604.

[4] M. Chaussidon, G. Libourel, Boron partitioning in the upper mantle: an experimental and ion probe study, Geochim. Cosmochim. Acta 57 (1993) 5053–5062.

[5] R. Hervig, G.M. Moore, L.B. Williams, S.M. Peacock, J.R. Holloway, K. Roggensack, Isotopic and elemental partitioning of boron between hydrous fluid and silicate melt, Am. Mineral. 87 (2002) 769–774.

[6] U. Hålenius, H. Skogby, M. Edén, S. Nazzareni, P. Kristiansson, J. Resmark, Coordination of boron in nominally boron-free rock forming silicates: evidence for incorporation of BO_3 groups in clinopyroxene, Geochim. Cosmochim. Acta 74 (2010) 5672–5679.

[7] A. Shariff, C. Nilsson, V. Auzelyte, M. Elfman, P. Kristiansson, K. Malmqvist, J. Pallon, M. Wegdén, The Lund nuclear microprobe sub-micron set-up. Part II: Beam line, focusing system and scanning, Nucl. Instrum. Meth. B 231 (2005) 7–13.

[8] M. Elfman, J. Pallon, V. Auzelyte, P. Kristiansson, K. Malmqvist, C. Nilsson, A. Shariff, M. Wegdén, The Lund nuclear microprobe sub-micron set-up. Part III: Sample stage, optical imaging and detector configuration in the experimental chamber, Nucl. Instrum. Meth. B. 231 (2005) 14–20.

[9] P. Golubev, P. Kristiansson, N. Arteaga-Marrero, M. Elfman, K. Malmqvist, E.J.C. Nilsson, C. Nilsson, J. Pallon, M. Wegdén, First results from the Lund NMP particle detector system, Nucl. Instrum. Meth. B 267 (12–13) (2009) 2065–2068.

[10] <http://www.vita.com/home/Learn/vmefaq/vmefaq.html> (03-12-2013).

[11] P. Kristiansson, M. Borysiuk, N. Arteaga Marrero, M. Elfman, E.J.C. Nilsson, C. Nilsson, J. Pallon, A pre-sample charge measurement system for quantitative NMP-analysis, Nucl. Instrum. Meth. 268 (2009) 1727–1730.

[12] M. Borysiuk, P. Kristiansson, L. Ros, N. Abdel, M. Elfman, E.J.C. Nilsson, J. Pallon, Evaluation of a setup for pNRA at LIBAF for applications in geosciences, Proceedings of of 21st IBA 2013, Submitted to Nucl. Instrum. Meth. B. 332 (2014) 202–206.

[13] K.A. Sjöland, P. Kristiansson, P. Tallone, Nuclear reaction analysis of boron for microbeam analysis of medical samples, Nucl. Instrum. Meth. B 104 (1) (1995) 255–260.